Turnover and storage of C and N in five density fractions from California annual grassland surface soils

W. T. Baisden[1] and R. Amundson
Ecosystem Sciences Division, Department of ESPM, University of California, Berkeley, Berkeley, California, USA

A. C. Cook
Center for Accelerator Mass Spectrometry, Lawrence Livermore National Laboratory, Livermore, California, USA

D. L. Brenner
Ecosystem Sciences Division, Department of ESPM, University of California, Berkeley, Berkeley, California, USA

Received 31 October 2001; revised 5 July 2002; accepted 31 July 2002; published 6 December 2002.

[1] We measured $^{14}C/^{12}C$ in density fractions from soils collected before and after atmospheric thermonuclear weapons testing to examine soil organic matter (SOM) dynamics along a 3 million year California soil chronosequence. The mineral-free particulate organic matter (FPOM; <1.6 g cm^{-3}) mainly contains recognizable plant material, fungal hyphae, and charcoal. Mineral-associated light fractions (1.6–2.2 g cm^{-3}) display partially or completely humified fine POM, while the dense fraction (>2.2 g cm^{-3}) consists of relatively OM-free sand and OM-rich clays. Three indicators of decomposition (C:N, $\delta^{13}C$, and $\delta^{15}N$) all suggest increasing SOM decomposition with increasing fraction density. The $\Delta^{14}C$-derived SOM turnover rates suggest that ≥90% of FPOM turns over in <10 years. The four mineral-associated fractions contain 69–86% "stabilized" (decadal) SOM with the remainder assumed to be "passive" (millenial) SOM. Within each soil, the four mineral-associated fractions display approximately the same residence time (34–42 years in 200 kyr soil, 29–37 years in 600 kyr soil, and 18–26 years in 1–3 Myr soils), indicating that a single stabilized SOM "pool" exists in these soils and may turn over primarily as a result of soil disruption. *INDEX TERMS:* 1615 Global Change: Biogeochemical processes (4805); 1694 Global Change: Instruments and techniques; 1803 Hydrology: Anthropogenic effects; 1851 Hydrology: Plant ecology; 9350 Information Related to Geographic Region: North America; *KEYWORDS:* Soil organic matter turnover, density fractionation, radiocarbon, stable isotopes, decomposition

Citation: Baisden, W. T., R. Amundson, A. C. Cook, and D. L. Brenner, Turnover and storage of C and N in five density fractions from California annual grassland surface soils, *Global Biogeochem. Cycles*, *16*(4), 1117, doi:10.1029/2001GB001822, 2002.

1. Introduction

[2] Hierarchies of chemical and physical bonding between soil organic matter (SOM) and mineral soil particles play a critical, and often dominant, role in determining whether the soil retains C inputs for a period of weeks, months, years, decades, centuries, or millennia [*Oades*, 1989, 1995; *Tisdall and Oades*, 1982; *Torn et al.*, 1997]. Of the world's major ecosystem types, grassland and agricultural systems best exhibit the control of soil structure, texture, and mineralogy over SOM dynamics [*Burke et al.*, 1989; *Carter*, 1996; *Kooistra and van Noordwijk*, 1996]. In fact, the two can provide a valuable contrast: grassland soils are noted for their high SOM contents and strong soil structure, while agricultural soils have lost considerable SOM compared to their uncultivated counterparts as a result of the destruction of soil structure via tillage [*Carter*, 1996; *Davidson and Ackerman*, 1993; *Elliott*, 1986].

[3] SOM can be restored to agricultural soil over a period of years by careful management including conservation tillage [*Beare et al.*, 1994; *Karlen and Cambardella*, 1996; *Lal and Kimble*, 1997]. Agricultural management for increased SOM may improve the productivity and function of agroecosystems, reduce nutrient losses from the system, and sequester C from atmospheric CO_2. In addition, the return of degraded agricultural land to grassland and forest systems presents similar benefits. While these possibilities are all beneficial, best management decisions require understanding of the processes controlling SOM storage and turnover.

[4] Many studies and reviews provide a useful conceptual understanding of the role soil structure plays in SOM

[1]Now at Landcare Research, Massey University, Palmerston North, New Zealand.

0886-6236/02/2001GB001822

storage and turnover [*Carter and Stewart*, 1996; *Oades*, 1989; *Tisdall and Oades*, 1982; *VanVeen and Kuikman*, 1990]. Nevertheless, these studies provide only a limited quantification of SOM turnover rates. Efforts to move toward a truly quantitative and predictive understanding are impeded by the complicated hierarchical nature of soil structure. That is, humic materials adhere to clay platelets to form small microaggregates, which are bound together with fine silt particles to form somewhat larger microaggregates. Successively larger mineral particles and aggregates are bound together as the binding agents change from humic materials to fine roots and fungal hyphae when aggregate sizes exceed ~200 μm [*Kooistra and van Noordwijk*, 1996; *Oades*, 1993, 1995; *Oades and Waters*, 1991]. Recently, methods have successfully utilized aggregate size and/or density to isolate SOM playing different roles in the aggregate hierarchy [e.g., *Beare et al.*, 1994; *Cambardella and Elliott*, 1993, 1994; *Golchin et al.*, 1995a, 1995b]. These methods describe the strength or type of mineral-organic association; the strongest mineral-organic bonds are believed to exist at the smallest scales and require the most energy to disrupt. Remaining methodological problems include: (1) comparability between different methods [*Carter and Gregorich*, 1996], and (2) failure of individual methods to yield reproducible results in different soil types [*Six et al.*, 2000]. Improved understanding of SOM dynamics requires greater characterization of the processes, which control the flow of SOM into and out of soil fractions with different degrees of mineral-association.

[5] To characterize the flows of SOM into and out of a series of detailed soil density fractions, we apply indices previously used to study SOM in whole soils or soil fractions. First, to characterize the processes responsible for the flow of SOM into mineral-associated SOM pools, we measure C:N, $\delta^{13}C$, and $\delta^{15}N$. These tracers generally reflect the degree of decomposition of SOM if the values of plant inputs to the soil remain constant [*Nadelhoffer and Fry*, 1988]. To quantitatively determine the rate at which SOM flows out of soil fractions, we apply radiocarbon from archived and contemporary samples as an isotopic tracer. Radiocarbon reflects decadal and millennial SOC turnover rates if a time series of samples spanning atmospheric "^{14}C-spike" can be analyzed [*Trumbore et al.*, 1996; *Trumbore*, 1993]. We utilize these element and isotope ratios in soils from a 3-million-year soil chronosequence in the eastern San Joaquin Valley, CA [*Harden*, 1987] to study the formation and turnover of stabilized SOM pools across a gradient of fertility and other soil properties appropriate to improving models of the terrestrial C cycle.

2. Methods

2.1. Sites

[6] Archived and contemporary samples were obtained from undisturbed sites on alluvial terraces formed by the Merced and Tuolumne Rivers, in the Eastern San Joaquin Valley, CA, USA [*Arkley*, 1962, 1964; *Harden*, 1987]. The soil parent material at all sites consisted of arkosic alluvium derived primarily from granodioritic rocks of the Sierra Nevada Batholith. All sites are in close proximity (25 km, see Table 1) and therefore have similar Mediterranean climate (hot, dry summers and cool, wet winters), with mean annual temperature of 16°C and mean annual precipitation of 300 mm [*Arkley*, 1962; *Brenner et al.*, 2001; *Harden*, 1987]. The Mediterranean climate supports a flora dominated by annual grasses and forbs, but with a secondary component of deep-rooted oaks that access deep water sources year-round at some sites (see Table 1). Plant species and functional group composition in California annual grasslands vary substantially from year to year, with a large biomass of N-fixing leguminous species in some years [*Jones and Woodmansee*, 1979].

[7] The availability of archived soils constrained the selection to terrace ages of <3, 200, 600 kyr, and 1–3 Myr. We attempted to sample modern sites adjacent to the archived sampling locations. Modern sampling locations were nearly identical for the 200 and 600 kyr sites, but the 3 Myr terrace was not sampled circa 1949 (see Table 1). Archived 1949 samples from a 1 Myr terrace provide a suitable substitute, but the 1 Myr soils were not resampled in 1997–1998 due to evidence of sheet-wash erosion and heavy grazing at these locations. Differences between the 1 and 3 Myr soils include subtle mineralogic differences in soil-parent material [*Marchand and Allwardt*, 1981] and greater depths to the duripan in the 3 Myr soil than the 1 Myr soil. The 1–3 Myr soils are assumed to be equivalent for this study. The surface horizon from the prebomb <3 kyr profile examined by *Baisden et al.* [2002] was too thick (28 cm) for comparison with other soil surface horizons and excluded from this study. While a similar (22–24 cm) comparison was performed for the 600 kyr soil, the <3 kyr soils may have contained contributions of allochthonous detrital SOM derived from recent alluvium with variable $\Delta^{14}C$ values. The <3 kyr comparison was therefore not appropriate given the expense of radiocarbon measurements. Specific information for each site appears in Table 1. More detailed data including profile descriptions can be found in the work by *Baisden et al.* [2002].

2.2. Soil Sampling and Preparation

[8] Archived and contemporary samples were collected from horizons identified in soil profiles. Contemporary soil pits were described and sampled according to standard methods [*Soil Survey Staff*, 1993], and similar procedures were followed for archived soils [*Arkley*, 1962, 1964; *Harden*, 1987]. The A1 and A2 horizons identified in contemporary profiles have similar properties (thickness, structure, etc.) across the chronosequence, and appear to be comparable to similar depth increments in archived soils. Deeper horizons do not necessarily have similar properties between sites. Details of field sampling and adjusted bulk density measurement appear in the work of *Baisden et al.* [2002].

[9] Contemporary soils were oven-dried (<50°C). Archived soil samples were stored in an air-dried state in glass jars, except for the 1978 sample that was stored in a paper can. This sample was examined for paper fragments using a dissecting microscope. Samples were passed though a soil splitter to obtain representative ~100 g samples for sieving to remove >2 mm material. Samples were then

Table 1. Information Describing the Sites Sampled

Soil Age/ Geologic Unit	Years Sampled	1997–1998 Location (Lat./Long.)	Vegetation	Soil Series	Surface Texture/ Parent Material Texture[a]	Parent Material Source	Distance from 1997–1998 Sampling	Reference (Archived Samples)
<3 kyr/Post-Modesto	1949 1978 1997	37.51384°N 120.46292°W	annual grassland/ oak savanna	grangeville	sandy loam/ sandy loam	recent floodplain alluvium derived from Sierra Nevada[b]	1 km 10 km ...	*Arkley* [1962] *Harden* [1987] ...
200 kyr/Riverbank (2)	1949 1978 1997	37.52°N 120.59°W	annual grassland	snelling	sandy loam/ sandy loam	glacial outwash alluvium derived from Sierra Nevada[b]	~10 m ~5 m ...	*Arkley* [1962] *Harden* [1987] ...
600 kyr/Turlock Lake	1952 1978 1997	37.62577° N 120.59085°W	annual grassland/ scattered oaks	cometa or montpellier	loamy sand/ loamy sand	glacial outwash alluvium derived from Sierra Nevada[c]	100 m 15 m	*Arkley* [1964] *Harden* [1987] ...
1 Myr/ North Merced Gravel	1949 1949	37.40°N 120.47°W	annual grassland	corning or redding	gravelly loam/ gravelly sandy loam	braided channel alluvium derived from Sierra Nevada and foothills[d]	~10 km ~11 km	*Arkley* [1962] *Arkley* [1962]
3 Myr/China Hat	1978 1998	37.464440°N 120.36906°W	annual grassland	corning or redding	gravelly loam/ gravelly sandy loam	braided channel alluvium derived from Sierra Nevada[e]	~200 m ...	*Harden* [1987] ...

[a] As inferred by *Harden* [1987], and similarly estimated for 1 Myr soil. Texture is for A horizon. Also see *White et al.* [1996] for detailed texture and mineralogy.

[b] Post-Modesto alluvium may contain a significant contribution from low-elevation watersheds composed of metasedimentary and volcanic rocks [*Harden*, 1987].

[c] The 200 and 600 kyr glacial outwash events are believed to punctuate episodes of alpine glaciation in high elevations of the Sierra Nevada [*Harden*, 1987]. Glaciated catchments at high elevation are dominated by the Sierra Nevada Batholith which have a granodioritic composition.

[d] Plio-Pliestocene deposits derived from uplift of the Sierra Nevada and believed to include greater contributions from metasedimentary and volcanic rocks of the foothills, including older terraces [*Marchand and Allwardt*, 1981]. These differences in mineralogy lead to exclusion of the 1 Myr sites from the ideal chronosequence [e.g., *Harden*, 1987; J. Harden, personal communication].

[e] Pliocene deposits derived from uplift of Sierra Nevada. <2 mm soil parent material is believed to be similar in texture and mineralogy to 200 and 600 kyr parent material [*Harden*, 1986; *White et al.*, 1996].

passed through a smaller soil splitter to obtain samples of 2–8 g for further analysis. Bulk soil samples (2–5 g) were ground in a corundum mortar and pestle to pass a 70-mesh sieve for C, N, and isotope analysis.

2.3. Density Fractionation

[10] Soils were subjected to a density fractionation procedure based on that of *Golchin et al.* [1994a, 1994b, 1995a, 1995b] to yield fractions listed in Table 2. Soils (4–8 g) were weighed into 50 mL polycarbonate centrifuge tubes and filled with 35 mL of 1.60 ± 0.03 g cm^{-3} sodium polytungstate (SPT) solution. The tubes were shaken gently end over end five times, and allowed to sit for 1 hour or more. The tubes were shaken gently again and the walls of the tube washed with an additional ~5mL of SPT from a wash bottle. The samples were then centrifuged to settle all particles >0.2 μm and <1.6 g cm^{-3}. After centrifugation, the floating FPOM fraction was aspirated onto a 7 cm quartz fiber filter (Whatman QM-A; prebaked 3hours at 850°C). Residual soil was resuspended in 35 mL of 1.60 ± 0.03 g cm^{-3} SPT, placed in an ice bath, and subjected to 6 min of ultrasonic disruption at 66% power and 50% pulse time on a Branson 350 sonifier with a 1/2-inch probe tip. For the last 10 s of sonication, the power was ramped to zero in order to assist the separation of light and dense particles [*Golchin et al.*, 1994b]. The floating <1.6 g cm^{-3} material comprised the first mineral-associated light fraction (MALF-1) and was aspirated onto a quartz filter as before. Subsequent mineral-associated light fractions (MALF-2 and MALF-3) were isolated in SPT of densities 1.85 ± 0.03 and 2.22 ± 0.05 g cm^{-3}, respectively. In each case, residual soil was resuspended by shaking, sonicated for 10 s at 20% power, and then the sonicator power was reduced to zero over another 10 s to enhance separation of organic material, which may have recombined with mineral particles. The suspensions were centrifuged and the floating material aspirated onto quartz filters as before. The residual >2.22 g cm^{-3} dense fraction (DF) was repeatedly resuspended, rinsed with deionized water (DI), and centrifuged again. Dissolved organic matter (DOM) lost to the SPT and DI was not recovered. Averaging across all soil samples, 11 ± 5% of the SOC in bulk soils was not recovered following fractionation, and is assumed to represent losses. However, for individual samples, the lost C is highly uncertain and therefore not reported.

[11] The DF was freeze-dried, and the FPOM and MALFs were freeze-dried if they did not air-dry during filtration. The mass of fractions collected on filters was calculated by subtracting the mass of the filter from the mass of the fraction on the filter. The FPOM and MALFs were ground to a fine powder in an SPEX 6800 cryogenic grinding mill, using stainless steel grinding tubes. The DF was ground in a corundum mortar and pestle to pass a 70-mesh sieve. Fractions were photographed prior to grinding using a Sony

Table 2. Description of the Fractions Separated From Soils

Fraction Abbreviation	Fraction Name	Density[a] (g cm^{-3})	Separated After Ultrasonic Disruption	Light Fractions	Mineral-Associated Fractions
FPOM	Free particulate organic matter	<1.60	no	X	
MALF-1	Mineral-associated light fraction (1)	<1.60	yes	X	X
MALF-2	Mineral-associated light fraction (2)	1.60–0.85	yes	X	X
MALF-3	Mineral-associated light fraction (3)	1.85–2.22	yes		X
DF	Dense fraction	>2.22	yes		X

[a] Densities separated in SPT prepared to ±0.03 g cm^{-3}.

DKC5000 digital camera mounted on a Leica M10 dissecting photomicroscope.

[12] One difficulty with the method was the tendency of the quartz filters to clog, thus limiting the amount of soil that could be processed. After grinding, the quartz filters also caused a blank problem for samples with very low C and N concentrations (discussed below). Therefore future researchers should attempt to avoid the use of quartz fiber filters for low OM-samples. *Cambardella and Elliott* [1993] present an alternative method.

2.4. Total C, N, and Isotope Analysis

[13] The $\delta^{13}C$ and $\delta^{15}N$ values as well as C and N content of most samples were determined using an elemental analyzer interfaced via continuous flow to an isotope ratio mass spectrometer (EA-CF-IRMS, Europa Scientific 20/20). The EA-CF-IRMS was calibrated to NIST 1547 Peach Leaves, assuming $\delta^{13}C = -25.9‰$ and $\delta^{15}N = +2.1‰$ for this material. Samples varied in C and N content, so a large suite of internal laboratory standards was used to correct each run for instrumental variation in observed $\delta^{13}C$ and $\delta^{15}N$ as a function of beam area. Reported $\delta^{13}C$ and $\delta^{15}N$ values were suitably bracketed by standards in both isotope ratio and measured beam area. Based on calibration runs for internal standards, we report an absolute precision relative to international isotope standards (NIST 8547 IAEA N-1, NIST 8540 PEF-1, and NIST 8542 ANU Sucrose) for this data set of approximately ±0.3‰ for $\delta^{15}N$ and ±0.15‰ for $\delta^{13}C$ (1σ error). Reported uncertainties are standard errors calculated either on the basis of replicate analyses or from the statistical fit of the calibration used to correct $\delta^{13}C$ or $\delta^{15}N$ as a function of beam area. Absolute precision can be neglected for comparison within the data set but should be added in quadrature to reported uncertainty when compared to other data sets.

[14] For most bulk samples, $\delta^{15}N$ and percentage of N were measured on a VG Optima EA-CF-IRMS at the USGS in Menlo Park, CA [*Baisden et al.*, 2002], using a procedure similar to that outlined above. The $\delta^{13}C$ and percentage of C of bulk samples were measured by dual inlet IRMS on a VG-Prism III at Lawrence Berkeley National Laboratory in conjunction with the analysis of ^{14}C samples as outlined below. Internal laboratory standards were used to demonstrate that data obtained from different instruments are generally comparable within reported uncertainty. Stable isotope data are presented in $\delta^{13}C$ and $\delta^{15}N$ notation, where differences in isotope ratios are given in part per thousand (‰) relative to the PDB standard for C isotopes and atmospheric N_2 for N.

[15] Samples for radiocarbon analysis were sealed in evacuated Vycor tubes with 0.5 g Cu, 1.0 g CuO, and a strip of Ag foil. These samples were combusted for 4 hours or more at 850°C, cooled at 1°C min^{-1}, and held for 2 hours at 650°C before further cooling. The CO_2, and in some cases N_2, were purified cryogenically [*Minagawa et al.*, 1984] using 13X molecular sieves to collect the N_2 gas at liquid nitrogen temperatures. CO_2 was converted to graphite for ^{14}C at the Center for Accelerator Mass Spectrometry (CAMS), Lawrence Livermore National Laboratory (LLNL). After purification, the quantities of CO_2 and N_2 released from the combustion of samples were measured manometrically. Radiocarbon data are presented in $\Delta^{14}C$ notation and include correction for stable isotope fractionation based on $\delta^{13}C$. The standard (0‰) represents approximately the $^{14}C/^{12}C$ ratio of the preindustrial atmosphere.

[16] For fractions <2.22 g cm^{-3}, percentage of C and percentage of N in the soil fractions are calculated by adjusting for the proportion of the quartz filter in the ground sample. We expected the quartz filters to be perfectly C- and N-free, but found a blank of 0.10 ± 0.03% C (n = 4) and 0.027 ± 0.010% N (n = 2). This background C and N was unimportant for most samples, but affects samples with low organic matter concentrations. Within the method outlined above, the high background appears after the filters are ground to a fine powder, suggesting that the blank may represent CO_2 and N_2 sorbed onto the surface of the finely divided silica either from the atmosphere, or from the liquid nitrogen bath in which the samples were ground in the SPEX mill. It is not clear that the full measured blank affects samples if OM coats the surfaces of the ground silica. Therefore we subtracted one-half of the blank concentration from all samples, and added one-half the blank concentration to estimates of uncertainty, which were carried through all subsequent calculations. Stable isotope ratios were not adjusted to account for the blank, and stable isotope data for samples with a high blank contribution (>∼10%) are not reported. For $\Delta^{14}C$, we recognized that the background could result in significant errors if it contained fossil-fuel-derived C with $\Delta^{14}C$ of −1000‰. Therefore the background $\Delta^{14}C$ was directly measured and a value of −150 ± 40‰ (n = 3) was derived. We incorporated this blank value into the $\Delta^{14}C$ values we report for the fractions and propagated the uncertainty.

[17] When necessary to obtain calculated results (by combining multiple horizons or using mass balance to calculate isotope ratios for a horizon by difference), mixing calculations were performed according to the equation $\delta_{1+2} = \delta_1 M_1 + \delta_2 M_2$ in which δ represents $\delta^{13}C$, $\delta^{15}N$, or $\Delta^{14}C$ values, and M represents mass for components 1 and 2 of the mixture. Uncertainties were propagated through all calculations using Gaussian error propagation rules, generally by adding the uncertainty or relative uncertainty in quadrature [*Bevington*, 1969]. In the final step of some calculations to obtain $\delta^{13}C$, $\delta^{15}N$, ^{14}C from mixing models, only the largest terms were included in the propagation of uncertainty. Propagated uncertainties represent one standard error.

2.5. Modeling $\Delta^{14}C$ to Estimate SOM Turnover Rates

[18] We estimated the turnover rate of SOM based on measured $\Delta^{14}C$ values using an approach similar to the box model presented in *Trumbore* [1993]. The approach recognizes that two "'pools" of SOM with different residence times can exist within the same soil or soil fraction. We assume one pool (C_{pool}) has annual to decadal residence times, while the other pool ($C_{passive}$) is passive (millennial turnover times). The model assumes that both pools have reached steady state (inputs = outputs). Starting in 1909, the model numerically incorporates C with a $^{14}C/^{12}C$ ratio derived from winter-growing (November-May) season-atmospheric CO_2 [*Berger*, 1987; *Levin and Kromer*, 1997; *Levin et al.*, 1994; *Nydal and Lovseth*, 1997; *Schonhofer*, 1992] into C_{pool} [for details, see *Baisden et al.*, 2002]:

$$\Delta C_{pool} = \left(I - kC_{pool}\right)\Delta t, \tag{1a}$$

$$\frac{\Delta\left(^{14}C_{pool}\right)}{\Delta t} = \left[A_{year-lag} I - (k+\lambda)^{14}C_{pool}\right]\Delta t. \tag{1b}$$

In these equations, C_{pool} and $^{14}C_{pool}$ represent SOC mass and ^{14}C mass in a portion of the soil fraction, while Δt represents a time step and is generally 1 year. An $A_{year\text{-}lag}$ is the $^{14}C/^{12}C$ ratio of the atmosphere corresponding to the subscript year, and is lagged by at least 1 year to represent the residence time of C in plant biomass and/or the residence time of SOC in "feeder" pools [*Gaudinski et al.*, 2000]. The decay constant for radiocarbon (λ) is set to 1.21×10^{-4} yr^{-1}. The $\Delta^{14}C$ of the passive pool was calculated based solely on radioactive decay (λ) and assumed age, and the $\Delta^{14}C$ of the modeled fraction is calculated as the mixture of the passive pool ($C_{passive}$) and C_{pool} in Equations (1a) and (1b) according to the following equation

$$\Delta^{14}C_{fraction} = \left(1 - P_{passive}\right)\Delta^{14}C_{pool} + P_{passive}\Delta^{14}C_{passive}, \tag{2}$$

where $P_{passive}$ is the proportion [$C_{passive}/(C_{passive} + C_{pool})$] of the density fraction, which is passive C.

[19] The model was implemented in Microsoft Excel with an annual time step. The values of k, lag, and $P_{passive}$ were optimized using Excel's "solver" application. The optimized fit minimized the sum of squared errors between the modeled and measured fraction $\Delta^{14}C$ obtained for each year a sample was available. In most cases, the summed error was zero (see Table 5). Figure 1 presents an example of a model fit. The measured $\Delta^{14}C$ data did not constrain both the passive SOM $\Delta^{14}C$ value ($\Delta^{14}C_{passive}$) and the lag time (*lag*). Variation of $C_{passive}$ residence times within a reasonable range (2000–5000 years) causes little variation in estimated parameter*s* using this approach. Therefore $\Delta^{14}C_{passive}$ was set to the middle of this range, −346‰ (equivalent to 3500 years), for consistency. This value was also consistent with passive SOM $\Delta^{14}C$ at similar depths in the model in *Baisden et al.* [2002].

[20] When only two samples (1949–1952 and 1997) were available, lag also was not constrained. Therefore lag for the FPOM was set to the account for the $\Delta^{14}C$ value measured for belowground biomass (Table 4). The lag was then estimated for MALFs based on the estimated residence time of FPOM and the $\Delta^{14}C$ value measured for belowground biomass (Table 4). To estimate error in model-derived estimates of turnover, a Monte Carlo simulation was performed for each fraction using 20 normally distributed simulated errors applied to measured $\Delta^{14}C$ values for the archived and contemporary samples (Table 4). Reported uncertainties in parameters derived from the model are the standard deviation of the solutions to the 20 Monte Carlo runs. These uncertainties result only from propagation of estimated analytical uncertainty in measured soil $\Delta^{14}C$ values, and do not include uncertainty from other sources including the $\Delta^{14}C$ of atmospheric CO_2.

3. Results

3.1. Photography

[21] The density fractions were examined using a dissecting microscope to establish that the expected variation in degrees of mineral association was observed across the spectrum of fractions. Typical photographs representing each density fraction appear in Figure 2. We observed marked visual differences between the lightest and densest fractions (FPOM and DF, see Table 2 for fraction descriptions), but more subtle differences among the MALF-1, MALF-2, and MALF-3 fractions. The FPOM consists almost entirely of recognizable plant debris (Figure 2a), as well as some active fungal hyphae. Fungal hyphae appear in association with surface plant debris (Figure 2a) and as apparent mycorrhizal associates of recently living plant root fragments (Figure 2b). Figure 2b illustrates that roots and root fragments may either appear exposed (lower), or coated with various organic and mineral particles (upper right). The FPOM fraction appears to play a role in macroaggregate formation, whereby smaller aggregates, mineral, and organic particles become bound together by roots and hyphae [*Tisdall and Oades*, 1982].

[22] The MALF-1, MALF-2, and MALF-3 (Figures 2c–2e) show large quantities of fine (<100 μm) particulate organic matter (POM) and lesser quantities of larger (>100 μm) POM. In most cases, the observable surfaces of the POM in the MALFs are partially or completely humified, in strong contrast to the FPOM fraction. Spores and pollen comprised the only recognizable plant materials in these fractions, and were generally found in the MALF-1 fraction. We also found charcoal and/or charred POM as a significant

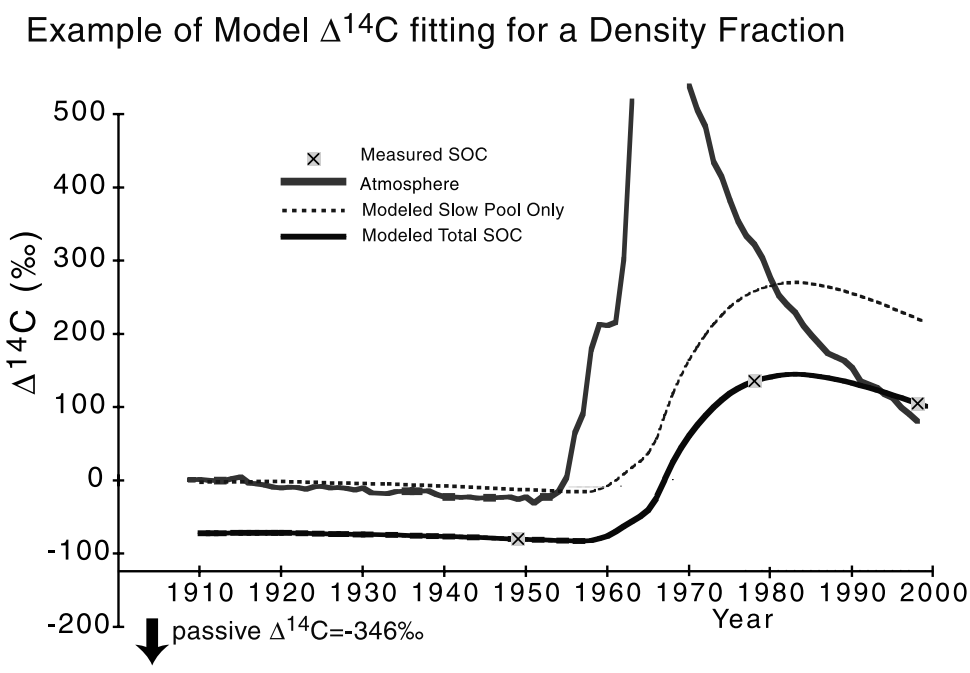

Figure 1. Model fit for $\Delta^{14}C$ in the MALF-3 in the ~0–11cm horizons of the 1949, 1978, and 1998 1–3 Myr soils. Data and parameters can be found in Tables 4 and 5, respectively.

component of the MALF-1, but not in the MALF-2 and MALF-3. The three MALFs also display a gradient of mineral content: the MALF-1 contained little mineral material, while the MALF-2 and MALF-3 contained increasing quantities of mineral material. In the case of the MALF-3, the quantity of mineral particles was sufficient to make observation of OM more difficult.

[23] The DF shows almost no evidence of organic matter in particulate form, but contains most of the SOM in two of the four soils examined (Figure 3). The DF fraction primarily consists of sand grains cleaned of surface coatings by sonication (Figure 2f). While the microscope did not allow examination of the surfaces of particles smaller than sands, an apparent visible OM-rich clay layer (Figure 2g) settled last during centifugation. Based on this, much of the OM in the DF appears to be sorbed on clay minerals.

[24] Overall, microscopic examination of the soil fractions suggests that increasing density can be considered equivalent to an increasing degree of mineral-organic association, combined with a progressive degree of decomposition of SOM. The former is consistent with an interpretation of similar fractions [*Golchin et al.*, 1995b].

3.2. Carbon and Nitrogen Storage in Density Fractions

[25] The proportions of total C and N in the different fractions varied widely and did not show a clear relationship with soil age (Figure 3 and Table 3). Figure 3 summarizes the data from Table 3 for the ~0–10 cm horizons. These data correspond to the A1 + A2 horizons sampled in contemporary soils, and the A1 horizons sampled in most archived soils. The standard errors plotted for the three 1–3 Myr soils (Figure 3) show that the method is reproducible within a given soil age class in samples 50 years collected apart and separated by up to 10 km. Compared to the 200 kyr and 3 Myr soils, the <3 and 600 kyr soils show much lower proportional C and N storage in the light fractions (LFs).

[26] The total magnitude of C and N storage within the LFs bear more similarity in the older soils, accounting for 700, 1000, and 800 g C cm^{-2} and 50, 100, and 60 g N cm^{-2} at the 200, 600 kyr, and 3 Myr sites, respectively. The youngest soil stores much more OM in LFs (3000 g C cm^{-2} and 280 g N cm^{-2}) than the older soils. Within the DF, the greatest C and N storage is found in the 3 Myr site with storage decreasing in the order <3, 200, 600 kyr, a trend that correlates with changes in soil texture from loam to loamy sand (Table 1). Overall, the relatively different patterns of C and N storage in the soil fractions observed as a function of soil age may be related to a matrix of factors that vary between sites, including surface soil texture, litter quality, and soil pH.

3.3. Indicators of Decomposition: C:N, $\delta^{15}N$, and $\delta^{13}C$

[27] We use C:N, $\delta^{15}N$, and $\delta^{13}C$ to investigate the processes responsible for the flow of OM into the soil fractions. These element and isotope ratios serve as indicators of the relative degree of microbial processing, which SOM has undergone before reaching its present state [*Nadelhoffer and Fry*, 1988].

[28] Generally, C:N (Figure 4) decreases with increasing density, while $\delta^{15}N$ (Figure 5), and $\delta^{13}C$ (Figure 6) values both increase with increasing degrees of mineral-organic association in the soil fractions. These results are consistent with a general increase in the degree of decomposition observed as a function of density. The observed trends in C:N ratios and $\delta^{13}C$ values are consistent with the results of *Golchin et al.* [1995b] for uncultivated sites.

[29] C:N data are presented for the sum of the contemporary A1 + A2 horizons (~0–10 cm depth) in Figure 4

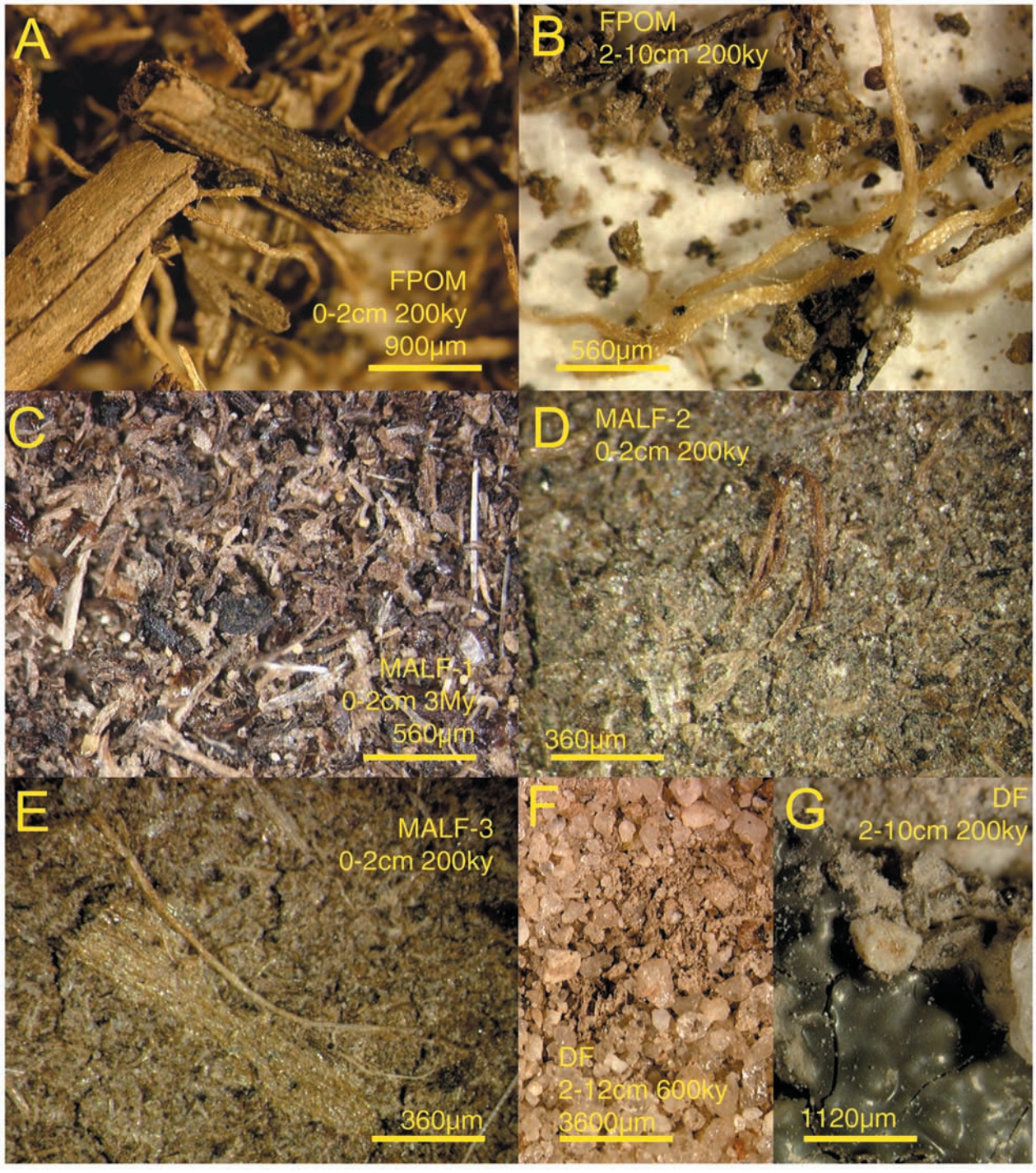

Figure 2. Digital images of soil fractions as described in frames A–G. The white background in (B) is the quartz filter.

because C:N ratio does not vary consistently with soil depth within a given soil fraction, except for the FPOM fraction which displays decreasing C:N with depth. The changing C:N of the FPOM is consistent with the lower C:N of belowground relative to aboveground plant parts. The marginally higher C:N observed for the MALF-1 relative to the FPOM fraction at some sites could result from the inclusion of chemically recalcitrant high C:N OM such as charcoal.

[30] The $\delta^{13}C$ and $\delta^{15}N$ values increase by 2–5‰ with increasing density at most sites (Figures 5 and 6). Surface soil (A1, 0–2 cm) FPOM is generally closest to above- and

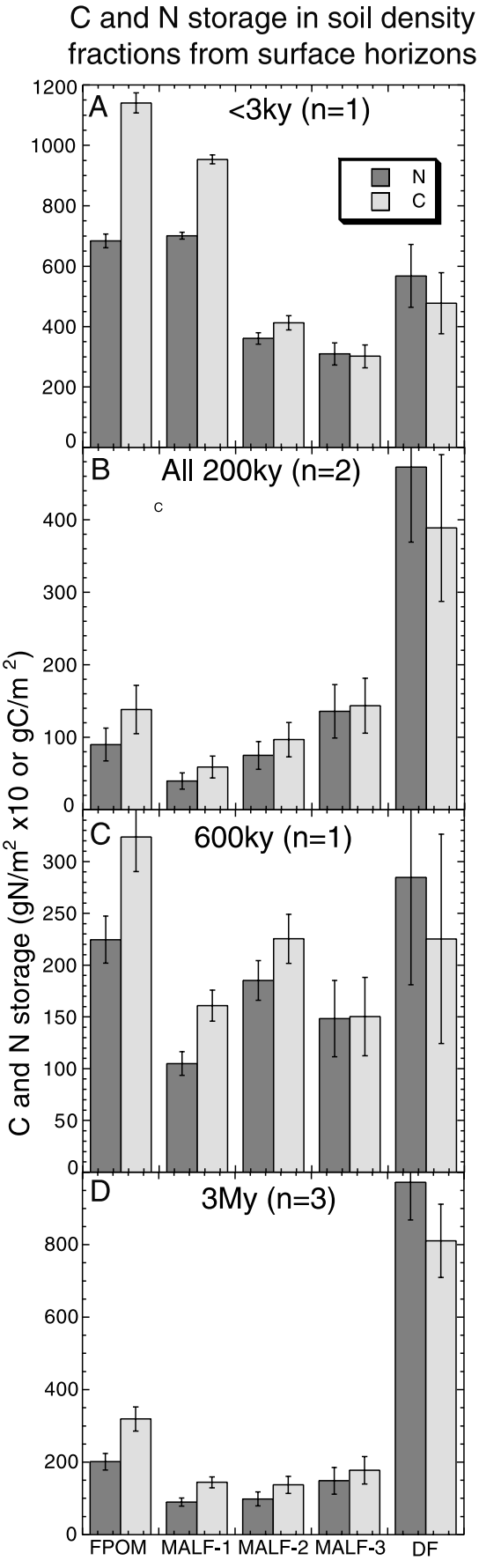

belowground plant values, while the MALF-3 and DF display the greatest ^{13}C and ^{15}N enrichment. Except in the <3-kyr soil, the deeper A2 SOM has higher $\bullet\delta^{13}C$ and $\delta^{15}N$ values than the A1 SOM. The pattern of $\delta^{13}C$ and $\delta^{15}N$ values observed across the density fractions did not vary systematically as a function of soil age. Patterns in plant and total SOM $\delta^{15}N$ values viewed as a function of soil age are discussed in *Brenner et al.* [2001].

3.4. $\Delta^{14}C$ and Estimated Turnover Rates

[31] To estimate passive SOM turnover rates, we measured $\Delta^{14}C$ in archived samples predating the pulse ^{14}C enrichment of atmospheric CO_2. In the 1949 samples, the measured $\Delta^{14}C$ values of density fractions (Table 4) decrease with increasing density, although not necessarily monotonically. The $\Delta^{14}C$ values for FPOM fractions in the 1949 200 kyr and 1 Myr samples closely match the 1949 atmospheric $\Delta^{14}C$, reflecting a decline of ~30–35‰ from preindustrial values due to ^{14}C-depleted fossil fuel C (the Suess effect). The lowest measured $\Delta^{14}C$ values occur in the 1949 1 Myr MALF-2 (−117 ± 6‰) and the 1952 600 kyr DF (−113 ± 4‰), and correspond to conventional ^{14}C ages of 900–1000 years.

[32] When available, surface soil samples from 1978 provide improved resolution of bomb ^{14}C incorporation in active and decadal SOM pools. All density fractions in the 1978 3 Myr soil display $\Delta^{14}C$ values greater than 100‰ (Table 4), suggesting the incorporation bomb-^{14}C during a period of 15–20 years. This 1978 3 Myr soil displays a marked decline in $\Delta^{14}C$ across the two lightest fractions, and a less pronounced decline across the remaining fractions. The $\Delta^{14}C$ value of the 1978 FPOM lags the estimated value for the 1978 atmosphere by approximately 20‰, suggesting a tight coupling between FPOM and atmospheric $\Delta^{14}C$ during this period when atmospheric $\Delta^{14}C$ decreased by roughly 20‰ per year.

[33] The contemporary samples had the highest $\Delta^{14}C$ values in MALFs (Table 4), suggesting that these fractions contain the largest proportions of decadal cycling pools that retain bomb ^{14}C. Within most fractions, the $\Delta^{14}C$ values of A1 (0–2 cm) horizons differ from those of A2 (~2–10 cm) horizons. This indicates that the upper 10 cm of soil is not well-mixed, a result that is consistent with the analysis of SOM transport performed by *Baisden et al.* [2002]. Beyond these observations, interpretation of contemporary $\Delta^{14}C$ values requires consideration of $\Delta^{14}C$ from comparable archived samples and numerical incorporation of the changes in the $\Delta^{14}C$ values of atmospheric CO_2. For this reason, we employ a two-box model (equations (1a), (1b), and (2)) to interpret the $\Delta^{14}C$ data for each soil fraction.

Figure 3. (opposite) C and N storage in surface horizons (a) 1997 <3 kyr soil 0–9 cm. (b) 1949 and 1997 200 kyr soil 0–10 cm. (c) 1997 600 kyr soil 0–12 cm. (d) 1949 1 Myr soil 0–8 cm, 1978 3Myr soil 0–9 cm, and 1997 3 Myr soil 0–11cm. In Figure 3a–3c, error bars indicate propagated uncertainties. In Figure 3d, error bars indicate standard errors calculated from the three replicates (1949, 1978, and 1998).

Table 3. C and N Storage in Soil Fractions

Soil Age	Sampled Year	Depth, cm	BD_{adj}, g cm^{-3}	N, g m^{-2}					N, g m^{-2}	C, g m^{-2}					C, g m^{-2}
				FPOM	MALF-1	MALF-2	MALF-3	DF	Bulk	FPOM	MALF-1	MALF-2	MALF-3	DF	Bulk
<3 kyr	1949	0–28	0.98	10.6 ± 2.4	28.6 ± 6.0	19.9 ± 4.2	25.2 ± 5.3	218.0 ± 33.8		175 ± 37	457 ± 94	269 ± 56	261 ± 54	2253 ± 368	4286 ± 620
<3 kyr	1997	0–2.5	0.86	32.3 ± 6.7	28.5 ± 5.9	4.8 ± 1.0	7.1 ± 1.5	12.3 ± 2.0	126.9 ± 18.3	569 ± 118	389 ± 80	52 ± 11	66 ± 14	107 ± 21	1271 ± 184
<3 kyr	1997	2.5–9	1.13	36.0 ± 7.5	41.5 ± 8.6	31.3 ± 6.5	23.8 ± 4.9	44.5 ± 7.3	214.3 ± 31.0	571 ± 118	565 ± 117	361 ± 74	236 ± 49	371 ± 72	2145 ± 310
<3 kyr	1997	9–22	1.32	4.1 ± 1.2	14.5 ± 3.1	6.5 ± 1.8	48.6 ± 11.1	104.6 ± 17.1	173.0 ± 25.0	64 ± 14	203 ± 42	88 ± 20	538 ± 115	968 ± 179	1694 ± 245
<3 kyr	1997	0–9		68.4 ± 10.0	70.1 ± 10.4	36.1 ± 6.6	31.0 ± 5.2	56.8 ± 7.6	341.2 ± 36.0	1141 ± 166	954 ± 142	413 ± 75	302 ± 51	478 ± 75	3417 ± 361
<3 kyr	1997	0–22		72.5 ± 10.1	84.5 ± 10.9	42.6 ± 6.8	79.5 ± 12.2	161.4 ± 18.7	514.2 ± 43.8	1205 ± 167	1157 ± 148	501 ± 78	840 ± 126	1445 ± 194	5110 ± 436
200 kyr	1949	0–10	1.24	7.7 ± 1.7	3.2 ± 0.8	5.5 ± 1.2	9.3 ± 2.0	47.1 ± 6.8		110 ± 23	49 ± 11	71 ± 15	98 ± 20	386 ± 55	878 ± 127
200 kyr	1949	10–41	1.12	2.5 ± 1.7	3.0 ± 1.6	5.5 ± 1.9	9.4 ± 2.5			72 ± 18	65 ± 16	91 ± 21	114 ± 25		312 ± 45
200 kyr	1997	0–2	1.05	4.9 ± 1.0	1.5 ± 0.3	3.6 ± 0.8	3.6 ± 0.8	7.8 ± 1.5	25.2 ± 3.6	87 ± 18	22 ± 5	48 ± 10	42 ± 9	67 ± 17	321 ± 46
200 kyr	1997	2–10	1.27	5.4 ± 1.2	3.2 ± 0.7	5.9 ± 1.3	14.2 ± 3.0	39.6 ± 7.6	71.1 ± 10.3	79 ± 16	46 ± 10	75 ± 16	147 ± 31	325 ± 83	762 ± 110
200 kyr	1997	10–29	1.63	2.8 ± 1.4	5.3 ± 2.4	2.5 ± 1.8	8.7 ± 2.4		92.9 ± 13.4	55 ± 14	83 ± 21	60 ± 16	119 ± 26	394 ± 56	777 ± 112
200 kyr	1997	0–10		10.3 ± 1.5	4.7 ± 0.8	9.5 ± 1.5	17.8 ± 3.1	47.4 ± 7.8	96.3 ± 10.9	166 ± 24	69 ± 11	123 ± 18	189 ± 32	392 ± 85	1083 ± 120
200 kyr	1997	0–22		13.1 ± 2.1	10.1 ± 2.5	12.0 ± 2.3	26.6 ± 3.9	47.4 ± 7.8	189.2 ± 17.3	222 ± 28	152 ± 23	182 ± 25	309 ± 41	786 ± 102	1860 ± 164
600 kyr	1949	0–20	1.8	3.8 ± 1.8	7.3 ± 2.2	2.9 ± 1.7	1.5 ± 1.8			71 ± 18	143 ± 31	−528 ± −150	−140 ± −70	684 ± 103	1307 ± 189
600 kyr	1997	0–2	1.08	16.0 ± 3.3	4.4 ± 0.9	3.9 ± 0.8	1.8 ± 0.4	3.4 ± 1.2	25.5 ± 3.7	234 ± 48	60 ± 12	48 ± 10	21 ± 4	28 ± 15	434 ± 63
600 kyr	1997	2–12	1.46	6.5 ± 1.5	6.1 ± 1.4	14.6 ± 3.1	13.1 ± 2.8	25.0 ± 8.0	106.4 ± 15.4	90 ± 19	101 ± 21	177 ± 37	130 ± 27	197 ± 100	822 ± 119
600 kyr	1997	12–24	1.58	1.5 ± 0.7	1.4 ± 0.7	1.5 ± 0.9	2.3 ± 0.9		50.4 ± 7.3	25 ± 7	30 ± 7	30 ± 8	31 ± 8	188 ± 27	336 ± 49
600 kyr	1997	0–12		22.4 ± 3.6	10.5 ± 1.7	18.5 ± 3.2	14.8 ± 2.8	28.5 ± 8.1	131.9 ± 15.8	324 ± 52	161 ± 24	225 ± 38	150 ± 28	225 ± 101	1256 ± 134
600 kyr	1997	0–22		23.9 ± 3.7	11.9 ± 1.8	20.0 ± 3.3	17.1 ± 3.0	28.5 ± 8.1	182.4 ± 17.4	349 ± 52	191 ± 25	256 ± 39	181 ± 29	413 ± 104	1592 ± 143
1 Myr	1949	0–7.6	1.26	9.7 ± 2.1	6.3 ± 1.4	3.6 ± 0.9	4.7 ± 1.1	72.0 ± 11.3		137 ± 28	96 ± 20	41 ± 9	55 ± 12	541 ± 100	910 ± 132
3 Myr	1978	0–9	1.224	38.8 ± 8.0	10.9 ± 2.3	14.7 ± 3.1	27.8 ± 5.8	117.8 ± 17.6		610 ± 126	168 ± 35	191 ± 40	319 ± 66	967 ± 156	2427 ± 351
3 Myr	1998	0–2	0.418	5.4 ± 1.1	4.7 ± 1.0	3.8 ± 0.8	7.5 ± 1.6	13.2 ± 1.9	35.4 ± 5.1	103 ± 21	75 ± 15	49 ± 10	87 ± 18	126 ± 19	481 ± 69
3 Myr	1998	2–11	1.408	6.4 ± 1.7	5.1 ± 1.4	7.6 ± 1.9	4.5 ± 1.4	88.5 ± 14.1	122.3 ± 17.7	108 ± 23	95 ± 20	131 ± 27	70 ± 15	798 ± 141	1198 ± 173
3 Myr	1998	11–40	1.34	2.6 ± 1.7	4.9 ± 1.9	1.6 ± 2.2	2.6 ± 2.0	202.5 ± 34.7	232.7 ± 33.6	40 ± 13	93 ± 22	36 ± 16	40 ± 15	1509 ± 337	1715 ± 248
3 Myr	1998	0–11		11.8 ± 2.0	9.7 ± 1.7	11.3 ± 2.0	12.1 ± 2.1	101.8 ± 14.2	157.6 ± 18.4	210 ± 31	170 ± 25	180 ± 29	157 ± 24	924 ± 143	1678 ± 187
3 Myr	1998	0–40		14.4 ± 2.6	14.6 ± 2.6	12.9 ± 3.0	14.7 ± 2.9	304.2 ± 37.5	390.3 ± 38.3	250 ± 34	263 ± 33	216 ± 33	198 ± 28	2434 ± 366	3393 ± 310

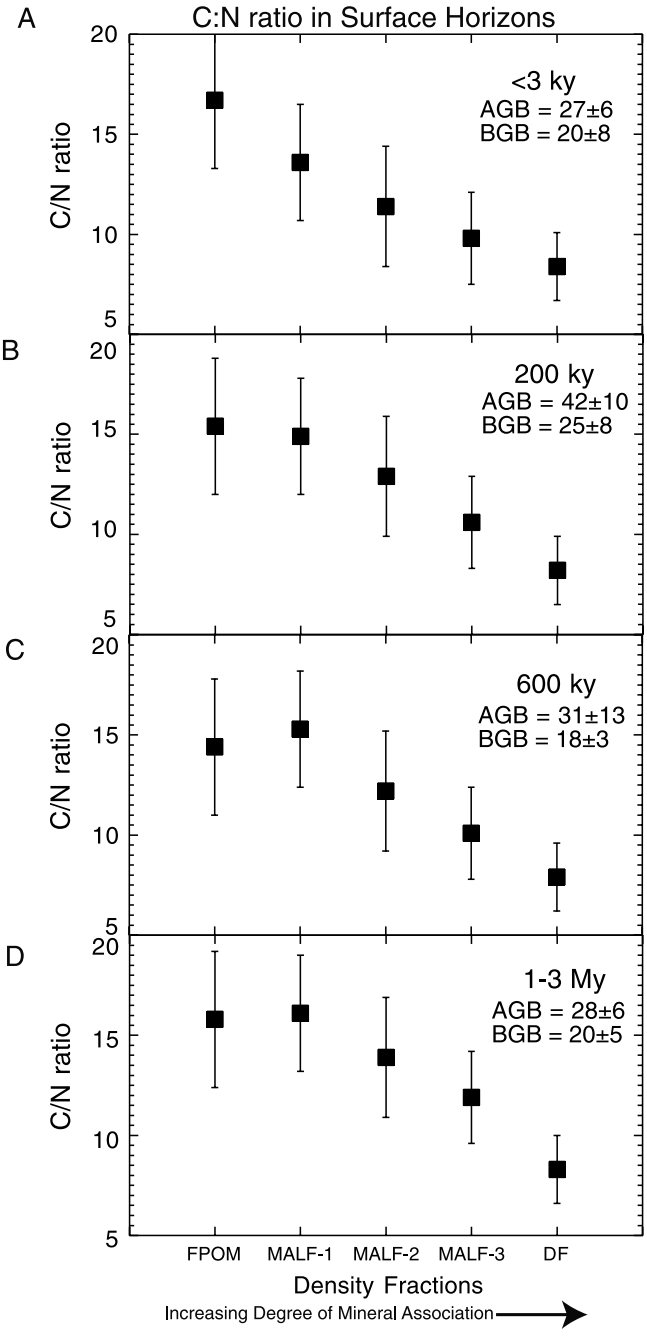

Figure 4. C:N ratio for soil density fractions from similar genetic horizons. (a) <3 kyr soil 0–9 cm sampled in 1997. (b) 200 kyr soil 0–10 cm sampled in both 1949 and 1997. (c) 600 kyr 0–12 cm sampled in 1997. (d) 1 Myr soil 0–7.6 cm sampled in 1949, 3 Myr soil 0–9 cm sampled in 1978, and 0–12 cm sampled in 1998. ABG and BGB are above- and belowground biomass, respectively.

[34] Model-derived results (Figure 7 and Table 5) suggest substantial differences in the turnover rates of FPOM and mineral-associated fractions (MALFs and DF). Most of the SOC in the FPOM fractions appear to have turnover rates of ~6 years or less. The residence times of C in FPOM are difficult to interpret using $\Delta^{14}C$ because they are short with respect to temporal variation in atmospheric $\Delta^{14}C$. Further, uncertainty results from variation in the $\Delta^{14}C$ values of aboveground plant material and belowground plant material and litter (Table 4).

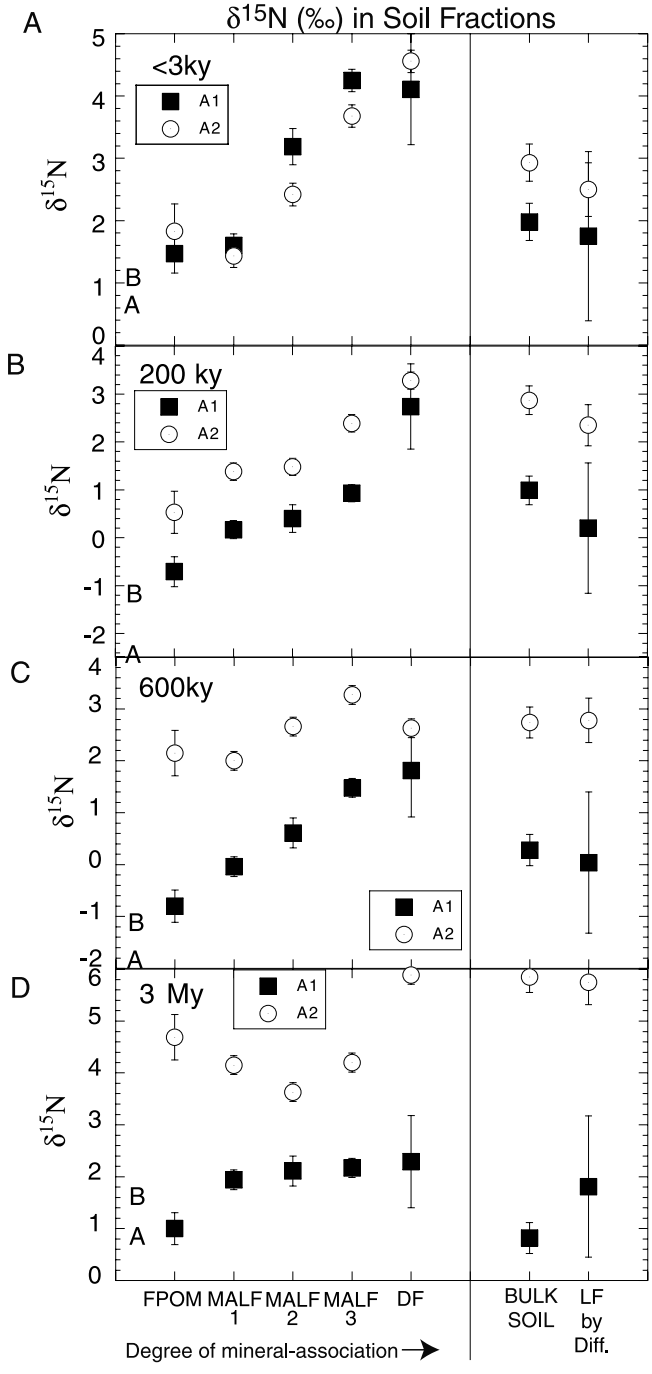

Figure 5. $\delta^{15}N$ in soil fractions for soils sampled in 1997–1998. (a) <3 kyr. (b) 200 kyr. (c) 600 kyr. (d) 3 Myr. The letters A and B plotted on the left side of each graph denote the $\delta^{15}N$ values of above- and belowground plant inputs, respectively. Bulk soil values are from *Brenner et al.* [2001]. A value for the sum of all light fractions (LF) was calculated by difference, to determine if simplified methods can be recommended.

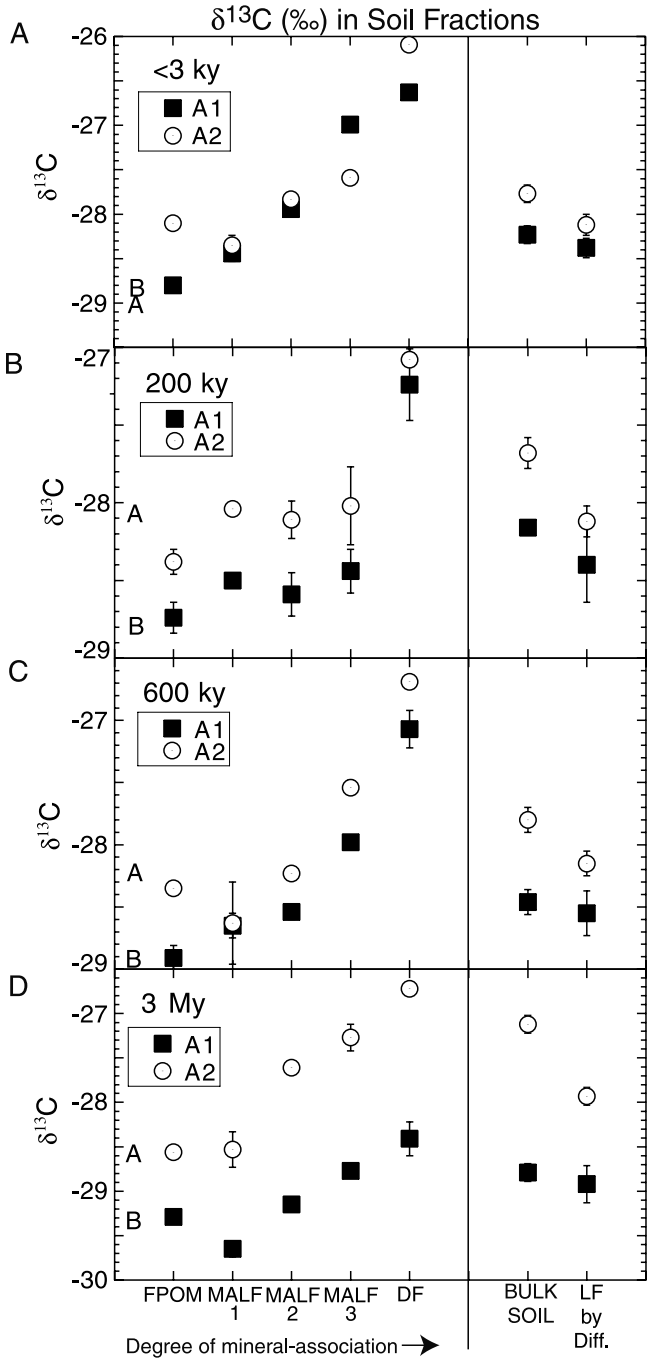

Figure 6. The $\delta^{13}C$ (‰) in soil fractions for soils sampled in 1997–1998. (a) <3 kyr. (b) 200 kyr. (c) 600 kyr. (d) 3 Myr. The letters A and B plotted on the left side of each graph denote the $\delta^{13}C$ values of above- and belowground plant inputs, respectively. A value for the sum of all light fractions (LF) was calculated by difference, to determine if simplified methods can be recommended.

[35] In contrast, we calculate well-defined residence times for mineral-associated fractions. The MALFs and DF display SOC turnover rates of 18–42 years for a calculated pool representing 69–86% of the total C in these fractions. Assuming a passive SOC pool with a residence time of 3500 years, passive SOC represents <10% of FPOM fractions and 14–20% of the MALFs, and 16–31% of the DF. In the 1–3 Myr soils, the residence times of MALF and DF appear to increase slightly with increasing density, although this trend is only marginally significant since error estimates do not include uncertainty in atmospheric $\Delta^{14}C$ and model assumptions. Mineral-associated fractions at other sites show no clear trend of residence time versus density.

[36] For each soil horizon, the passive SOM pool can be viewed as 14–31% of the C in the MALF and DF plus a small amount (<10%) of C in the FPOM. Similarly, 69–86% of C in the MALF plus DF describes the stabilized (decadal) SOM pool, and the remainder of SOC represents the active pool. In this sense, active SOM includes both the 90–99% of FPOM with residence times <6 years and any DOM lost to the SPT and DI-water rinses during density fractionation. We suggest that these interpreted active, stabilized, and passive pools correspond to the three pools of SOM considered in ecosystem biogeochemistry models [*Jenkinson*, 1990; *Parton et al.*, 1987, 1996] and found by modeling $\Delta^{14}C$ as a function of depth [*Baisden et al.*, 2002].

[37] Examining model-derived parameters (Figure 7 and Table 5) for these three pools in the 200, 600 kyr, and 3 Myr soils, neither the fraction of passive SOC in the isolated fractions nor the C residence time in FPOM appear to vary consistently as a function of soil age. However, the residence time of the stabilized SOC pool suggests decreasing residence times as a function of soil age. This trend primarily results from more rapid turnover in the 3 Myr soil. The 600 kyr soil does not appear to differ significantly from the 200 kyr soil in stabilized SOC residence time, but the greater sampling depth in the 1952 600 kyr sample hinders this comparison. Based on *Baisden et al.* [2002], the most likely effect of calculating turnover rates based on a deeper sampling interval is an increase in the observed residence times, due to the inclusion of older SOC at depth. Given this, the calculated stabilized SOC pool residence times appear to decrease with soil age in a manner consistent with the residence times calculated in *Baisden et al.* [2002].

4. Discussion

4.1. Density Fractionation Procedures

[38] The density fractionation procedures presented here separate soil fractions in which the degree of mineral-organic association increases with increasing density. In most cases, C:N, $\delta^{15}N$, and $\delta^{13}C$ indicate that the degree of SOM decomposition increases with increasing density. Yet, stabilized (decadal) SOM with similar calculated turnover rates exists within all mineral-associated fractions from a given soil sample. Thus these procedures yield useful fractions for understanding SOM cycling and calibrating terrestrial ecosystem biogeochemistry models.

[39] However, the number of fractions may be larger than needed to develop reliable estimates of C pools and residence times. Can the density fractionation procedures be simplified to yield fewer fractions and retain a similar understanding of C cycling? Currently, ^{14}C studies of SOM turnover rely on a mixture of chemical and physical fractionation methods

Table 4. Measured $\Delta^{14}C$ Values for Soil Fractions

Soil Age	Sampled Year	Depth, cm	$\Delta^{14}C$ FPOM	MALF-1	MALF-2	MALF-3	DF	Bulk	$\Delta^{14}C$ by Difference LFs	MALFs
200 kyr	1949	0–10	−36.9 ± 4.6	−57.6 ± 5.5	−65.2 ± 5.9	−65.6 ± 4.7	−71.3 ± 3.9	−61.9 ± 4.1	−54.5 ± 5.8	−59.6 ± 7.6
200 kyr	1949	10–41								
200 kyr	1997	0–2	105.8 ± 4.9	114.5 ± 5.2	132.0 ± 5.1	118.0 ± 4.7	83.8 ± 4.8	110.8 ± 5.0	117.9 ± 9.9	124.2 ± 15.2
200 kyr	1997	2–10	134.9 ± 5.7	99.7 ± 5.9	94.3 ± 5.3	97.9 ± 5.1	90.3 ± 4.8	118.7 ± 5.4	139.8 ± 10.3	140.9 ± 12.6
200 kyr	1997	10–29					−34.4 ± 4.5	−6.4 ± 6.3	22.4 ± 8.7	
200 kyr	1997	0–10	119.6 ± 4.3	104.5 ± 4.4	109.0 ± 4.6	102.4 ± 4.2	89.2 ± 4.1	116.4 ± 4.1	133.6 ± 7.9	137.2 ± 10.0
200 kyr	1997	0–22								
600 kyr	1949	0–20	−53.0 ± 11.5				−112.5 ± 4.1	−88.2 ± 4.1	−61.5 ± 5.8	−62.6 ± 6.7
600 kyr	1997	0–2	147.2 ± 5.1	144.1 ± 5.2	148.7 ± 4.6	91.2 ± 6.1	54.9 ± 4.4	144.8 ± 5.1	151.0 ± 6.7	156.0 ± 17.3
600 kyr	1997	2–12	161.4 ± 5.2	112.6 ± 5.4	127.8 ± 4.7	114.2 ± 4.6	68.7 ± 4.9	135.4 ± 5.0	156.5 ± 14.0	155.7 ± 16.4
600 kyr	1997	12–24					−34.4 ± 3.7	−11.7 ± 4.4	17.0 ± 6.6	17.0 ± 6.6
600 kyr	1997	0–12	151.2 ± 4.0	124.3 ± 4.5	132.2 ± 4.0	111.0 ± 4.1	67.0 ± 4.5	138.6 ± 3.7	154.5 ± 9.3	155.9 ± 13.3
600 kyr	1997	0–22					35.3 ± 7.1	112.5 ± 4.9	139.2 ± 9.9	137.9 ± 14.0
1 Myr	1949	0–7.6	−35.2 ± 4.2	−62.4 ± 4.2	−116.5 ± 5.6	−80.5 ± 5.0	−86.6 ± 3.7	−66.2 ± 5.0	−36.3 ± 7.3	−37.0 ± 11.8
3 Myr	1978	0–9	338.8 ± 6.6	217.1 ± 5.4	154.4 ± 4.8	135.3 ± 4.6	113.3 ± 4.5	199.2 ± 5.2	256.1 ± 15.4	196.8 ± 26.9
3 Myr	1998	0–2	106.1 ± 4.2	170.0 ± 5.5	157.4 ± 5.2	140.5 ± 5.1	123.3 ± 5.1	125.7 ± 5.2	126.6 ± 7.3	134.9 ± 10.4
3 Myr	1998	2–11	128.1 ± 10.1	106.9 ± 6.5	96.5 ± 5.5	59.8 ± 7.7	78.1 ± 5.8	91.7 ± 5.4	118.9 ± 8.3	115.5 ± 11.9
3 Myr	1998	11–40					−45.9 ± 3.8	−27.7 ± 4.5	105.8 ± 7.2	105.8 ± 7.2
3 Myr	1998	0–11	117.4 ± 5.8	134.6 ± 6.3	113.2 ± 5.5	104.6 ± 7.5	84.3 ± 5.2	101.4 ± 4.4	121.0 ± 6.4	122.2 ± 8.9

[*Paul et al.*, 1997; *Trumbore et al.*, 1996; 2000; *Trumbore and Zheng*, 1996], which are not clearly linked to the chemical or physical nature of SOM. Recent work [*Gaudinski et al.*, 2000; *Trumbore*, 2000] accepts this difficulty, and attempts to discern the pool structure of SOM by including $\Delta^{14}C$ measurements of soil respiration. The density methods presented here allow isolation of SOM fractions, which when interpreted with models and assumptions, describe pools of C commonly used in ecosystem biogeochemistry models [*Parton et al.*, 1996].

[40] The number of measured fractions can be reduced if the $\Delta^{14}C$, $\delta^{15}N$, $\delta^{13}C$ for a fraction is calculated by difference based on mass balance. Difference calculations were performed and plotted on the right sides of Figures 5–7. These difference calculations produce results for $\delta^{13}C$, which differ significantly from bulk $\delta^{13}C$ values, and roughly match average values for LF and the three MALFs. For $\delta^{15}N$ and $\Delta^{14}C$, the same comparison yields inconsistent or uncertain results. The relative uncertainty increases in difference calculations due to the inclusion of the uncertainty in the two or more measurements in the value calculated. Additionally, bias may result from the failure to account for DOM lost to the SPT and DI-water rinses during density fractionation. Therefore difference calculations are only reliable if isotope ratios of fractions can be measured precisely and DOM is considered part of the SOM pool, which is calculated by difference.

[41] For stable isotope measurements, the full suite of fractions measured here is recommended due to the pattern of $\delta^{13}C$ and $\delta^{15}N$ observed across the full density spectrum (Figures 5 and 6). However, based on the similar $\Delta^{14}C$-derived turnover rates of the mineral-associated fractions (Figure 7), it appears that the three MALFs and perhaps the DF can be combined for radiocarbon measurement. Given the distinct turnover rates of FPOM and mineral-associated fractions, separation of FPOM (<1.6 g m^{-3}) remains critical for isolating SOM fractions stabilized by soil structure [*Trumbore*, 1993]. The detailed fractions isolated here suggest that a density cutoff of ~1.6 g cm^{-3} may more effectively separate FPOM from mineral-associated SOM than density separations at ~2.0 g cm^{-3}. Perhaps most importantly, the physical isolation of FPOM (1.6 g cm^{-3}) (which contains much of the active C) permits mathematical separation (equation (2), Table 5, and Figure 7) of stabilized and passive SOM pools within mineral-associated fraction(s) when a time series of samples is available. This mathematical

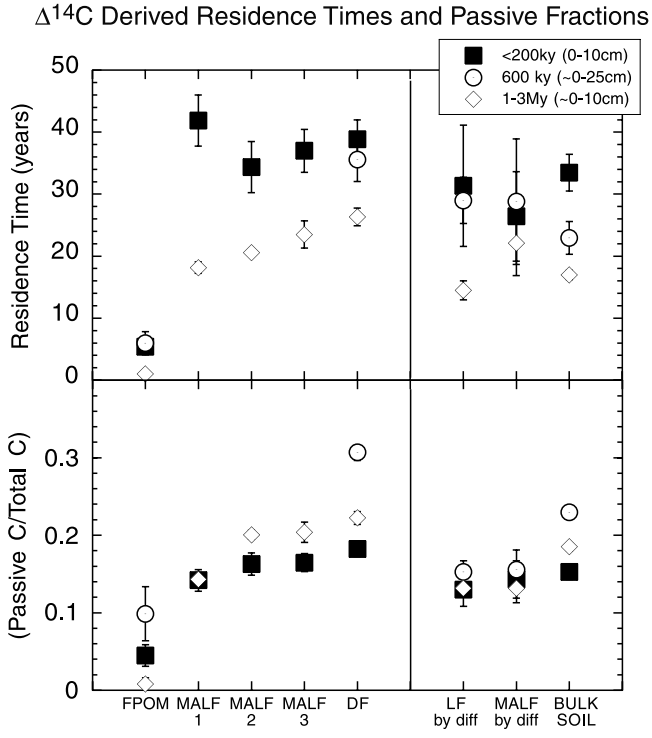

Figure 7. (a) Turnover times derived for C pool (in equations (1) and (2)) based on $\Delta^{14}C$ measurements. (b) The proportion of passive SOC to total SOC ($C_{passive}/[C_{pool} + C_{passive}]$ in Equations (1) and (2)) based on $\Delta^{14}C$ measurements.

Table 5. $\Delta^{14}C$ Derived Parameters Describing SOM Turnover

		Lag Time, years	Turnover Time, years	Proportion Passive[a]	Sum of Squared Error, ‰
200 kyr	FPOM	1.0	15.4 ± 0.8	10.05 ± 0.01	10.00
200 kyr	MALF-1	3.0	41.9 ± 4.1	0.14 ± 0.01	0.00
200 kyr	MALF-2	3.0	34.4 ± 4.1	0.16 ± 0.01	0.00
200 kyr	MALF-3	3.0	37.0 ± 3.5	0.16 ± 0.01	0.00
200 kyr	DF	3.0	38.9 ± 3.1	0.18 ± 0.01	0.00
200 kyr	Bulk	3.0	33.5 ± 3.0	0.15 ± 0.01	0.00
200 kyr	LFs by diff.	3.0	31.4 ± 9.8	0.13 ± 0.02	0.00
200 kyr	MALFs by diff.	3.0	26.4 ± 7.2	0.14 ± 0.02	0.00
600 kyr	FPOM	6.5	6.0 ± 1.9	0.10 ± 0.03	0.00
600 kyr	MALF-1				
600 kyr	MALF-2				
600 kyr	MALF-3				
600 kyr	DF	8.0	35.6 ± 3.5	0.31 ± 0.01	0.00
600 kyr	Bulk	8.0	22.9 ± 2.6	0.23 ± 0.01	0.00
600kyr	LFs by diff.	8.0	29.0 ± 3.7	0.15 ± 0.01	0.00
600 kyr	MALFs by diff.	8.0	28.8 ± 10.1	0.16 ± 0.02	0.00
3 Myr	FPOM	2.0 ± 0.3	1.0	0.01 ± 0.01	25.35
3 Myr	MALF-1	1.5 ± 1.2	18.1 ± 0.9	0.14 ± 0.01	0.00
3 Myr	MALF-2[b]	13.0 ± 0.0	6.8 ± 0.2	0.29 ± 0.00	9.12
3 Myr	MALF-2[c]	3.8 ± 0.5	20.6 ± 0.4	0.20 ± 0.01	0.00
3 Myr	MALF-3	3.1 ± 1.7	23.5 ± 2.2	0.20 ± 0.01	0.00
3 Myr	DF	1.4 ± 1.1	26.3 ± 1.4	0.22 ± 0.01	0.00
3 Myr	Bulk	1.0 ± 0.0	17.0 ± 0.7	0.19 ± 0.01	12.15
3 Myr	LFs by diff.	1.0 ± 0.0	14.5 ± 1.5	0.13 ± 0.01	26.47
3 Myr	MALFs by diff.	1.0 ± 0.9	22.1 ± 5.2	0.13 ± 0.02	25.70

[a] Assumes the residence time of passive C to be 3500 years.
[b] This fit was deemed unreasonable. The 1949 $\Delta^{14}C$ value (−116‰) was unusual.
[c] This fit replaces * by fitting 1978 and 1998 data only.

separation represents an alternative method to acid hydrolysis [*Trumbore and Zheng*, 1996]. However, these recommendations should be viewed with caution for soils unlike those studied, as density fractionation can yield results highly dependent on soil mineralogy [*Six et al.*, 2000].

4.2. Conceptual Model: Decadal Stabilization of SOM

[42] The indicators of decomposition ($\delta^{13}C$, $\delta^{15}N$, and C:N; Figures 4–6) vary systematically across the density fractions representing a gradient of mineral-organic association. In contrast, $\Delta^{14}C$-derived stabilized SOC residence times vary little across the same MALF and DF fractions. This contrast can be explained by recognizing that the degree of SOM decomposition reflects the processes occurring before or during the inflow of OM to the isolated fraction, while the $\Delta^{14}C$-derived residence times describe the rate of flow through each fraction. Given this logic, we propose a conceptual model (Figure 8) that is consistent with our observations.

[43] Our conceptual model assumes that plant debris enters the FPOM pool. Because this fraction has little mineral material, few decomposition products are preserved. But as decomposition proceeds, fungal hyphae and bacterial cells begin to bind mineral particles to the organic debris. As the organic matter becomes humified, the number of carboxylic groups on OM surfaces increase, facilitating strong bonds to negatively charged clay particles via multivalent cation bridges [*Oades*, 1989]. At this point, mineral particles begin to protect microbial debris and humified POM from further microbial attack. Decomposition proceeds with preservation of humified debris until the physical protection of the remaining OM from microbes is complete. During the stage in which some decomposition products are preserved by mineral-organic associations, decomposition within a parcel of OM may be expected to follow a Rayleigh distillation model [*Amundson and Baisden*, 2000; *Nadelhoffer and Fry*, 1988] in which a proportion, P, of the original FPOM substrate is preserved, and the ^{13}C- and ^{15}N-depleted metabolic products (primarily CO_2 and inorganic N compounds) are removed. C:N will also decrease if microbial products, which have lower C:N than FPOM, are preserved. If *P* is related to the particle size of the preserved OM, which becomes coated with mineral particles, then it follows that microaggregates with low *P* will have a small amount of OM preserved among abundant mineral particles, leading to separation at high density (or vice versa). The concept of Rayleigh distillation is consistent with visual observation (Figure 2) the MALFs appear to contain individual fragments of POM and associated mineral particles, with MALF-1 dominated by organic debris, and MALF-2 and MALF-3 displaying increasing quantities of mineral material, and smaller OM fragments.

[44] However, some processes do not fit this simple model. These processes are represented by the "square pegs" in Figure 8, and include apparent preservation of POM with tough organic coatings, such as spores, pollen, and seeds (Figure 2c). Charcoal, charred plant debris, and lignin coils may also be included in this category. The resistant organic surfaces of these materials appear to prevent strong mineral-organic bonds, and these types of OM therefore appear in the MALF-1 [see *Golchin et al.*, 1994b] although they generally represent <20% of this fraction in the soils examined here by microscopic inspection. As indicated in Figure 8, the fate of these materials in soil is not well understood. Preservation of a higher proportion of these "square pegs" by *Golchin et al.*'s [1994b]

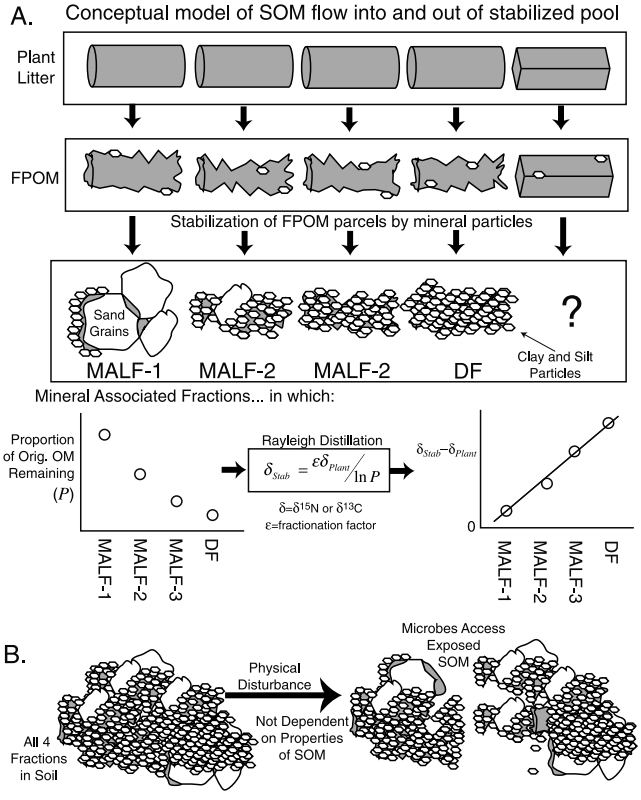

Figure 8. Conceptual model for the flow of OM into and out of mineral-associated fractions. (a) The inflow of OM begins when plant litter enters FPOM. Batches of FPOM become coated by mineral particles, which preserve decomposition products and protect OM from further decomposition. The proportion of the original OM remaining determines the particle size of mineral-associated OM, and therefore the density of the OM + mineral particles after ultrasonic disruption. If the decomposition of individual FPOM parcels follows a Rayleigh Distillation model, then denser fractions have higher $\delta^{13}C_{Stab}$ and $\delta^{15}N_{Stab}$. The last column of input material represents "square pegs" which are discussed in the text. Note that sand-sized particles are isolated in the DF, while they may have contributed to physical protection of MALF OM. (b) All four mineral-associated fractions exist together in soil and decompose primarily when released from physical protection by disturbances such as root growth, burrowing, etc.

^{13}C-NMR study might account for the abundant aromatic and alkyl C observed in this fraction and assumed by Golchin et al. to indicate a high degree of decomposition.

[45] This model of stabilized SOM formation is not consistent with the model proposed by *Golchin et al.* [1994a]. They suggest that FPOM enters the MALF-3 upon encrustation by mineral particles and then undergoes further decomposition. The ongoing decomposition results in the creation of parcels of occluded highly decomposed OM (from MALF-2 to MALF-1) and strongly mineral-associated OM (DF). This pathway of stabilized SOM formation would be interpreted to result in an increase in C/N, ^{13}C, and ^{15}N as well as Δ^{14}C-derived lag times in the order FPOM → MALF-3 → MALF-2 → MALF-1. This progression is not observed in the soils examined here. Instead, we observe a simpler pattern and therefore propose that this alternative model for stabilized SOM formation and turnover may be applied to SOM turnover at regional and global scales.

4.3. Implications of Conceptual Model: Variations in Stabilized SOM Turnover Across Environmental Gradients

[46] It has been hypothesized that the turnover of stabilized SOM occurs when aggregates are disrupted, exposing OM surfaces to decomposer activity [*Oades*, 1989, 1993, 1995; *Tisdall and Oades*, 1982; *VanVeen and Kuikman*, 1990]. Direct physical disturbance of soil aggregate structure results in the mineralization of large quantities of C and N by soil microorganisms [*Beare et al.*, 1994]. Moreover, much of the early success of temperate agriculture can be attributed to the release of physically protected soil-organic nutrients by mechanical tillage over decadal timescales, although the ongoing release of soil-organic nutrients can result in the depletion of the stabilized SOM pool's nutrient reservoir [*Tiessen et al.*, 1994].

[47] Mechanisms for the physical disruption of soil aggregates (as shown in Figure 8b) include root growth, penetration by fungal hyphae, activity of burrowing fauna, shrink/swell or freeze/thaw, and mechanical tillage. With the possible exception of fungal hyphae, these mechanisms seem unlikely to be directed at any particular soil fraction. If all fractions are disrupted equally, stabilized SOM within them experiences the same probability of exposure from physical protection, and therefore has similar residence times (as shown in Figure 7a).

[48] The hypothesis that the disruption of soil structure drives the mineralization of stabilized SOM appears to be consistent with stabilized SOC residence times that decrease as soil age increases. This observation is a very important result, because mineral-associated SOM is the dominant SOC pool in the horizons studied, yet the apparent trend cannot be explained by generally accepted arguments that SOC residence times are a function of soil clay content or climate [*Anderson and Paul*, 1984; *Burke et al.*, 1989; *Parton et al.*, 1987]: the 1–3 Myr soils have the highest clay (field textures indicated 8–10% clay at 200 kyr, 5–8% clay at 600 kyr, and 10–15% at 1–3 Myr in agreement with *Harden* [1987]) but shortest stabilized SOC residence times, and the soils experience similar climate. Assuming that plants allocate more C to growth of roots and mycorrhiza as soil-nutrient availability decreases [*Landsberg and Waring*, 1997], higher rates of stabilized SOM turnover in the 1–3 Myr soils could be related to increased root and mycorrhizal activity as a result of decreased N and P availability in highly weathered soils [*Baisden et al.*, 2002]. If supported by further research, this hypothesis suggests that, in addition to mechanisms of physical soil disturbance, terrestrial ecosystem biogeochemistry models should consider feedbacks between plant C allocation to roots and stabilized SOM turnover rates.

[49] The following caveats apply to the conceptual model and hypothesized relationship between stabilized SOM

turnover and plant belowground C allocation. First, density fractionation results can vary considerably between soils with different mineralogies [*Six et al.*, 2000], so caution is advised in applying these concepts to soils that are different from those studied. Despite this, soils derived from granitic alluvium were selected to be representative of typical continental environments and represent a substantial weathering gradient [*White et al.*, 1996]. In addition, the turnover times obtained from density fractionation are supported by a largely independent method [*Baisden et al.*, 2002]. Second, these results are representative of soil aggregration at scales <2 mm but may not incorporate larger scale soil structure. Larger scale soil structure may be important when roots, colloids, and dissolved OM regularly pass through limited pore space or cracks between aggregates rather than soil volume as a whole [*Kooistra and van Noordwijk*, 1996]. We observed this phenomenon in horizons below 20 cm, and therefore note that the active zone of SOM cycling may be concentrated within "hot spots" in some soils and soil horizons. Large-scale separation of "hot spots" from zones of inactivity could lead to differences in stabilized SOM residence times.

[50] In summary, the conceptual model, as drawn in Figure 8, implies the following for models of SOM turnover. Lag times (Equation (1a) and Table 5) suggest that these pathways of stabilized SOM formation are not prolonged, and that stabilized SOM does not progress through a series of stages. Despite this, stabilized SOM may form by a variety of pathways involving varying degrees of preservation of the original organic matter input. The stabilized pool remains physically protected until disturbance occurs. Research and models of SOM should consider the possibility that stabilized SOM turnover is linked to belowground plant allocation as well as other physical disturbance mechanisms.

5. Conclusions

[51] We separated five soil-density fractions, which display clear differences in the properties of SOM contained within them. All three indicators of decomposition (C:N ratio, $\delta^{13}C$, and $\delta^{15}N$) suggest higher degrees of SOM decomposition with increasing density across the soil fractions. SOM turnover rates derived from $\Delta^{14}C$ measurements suggest that FPOM contains $\geq$90% active SOC which turns over much more quickly than SOM in the mineral-associated fractions. The four mineral-associated fractions contain 69–86% stabilized (decadal) SOC with the remainder assumed to be passive (millennial) SOC with a residence time of ~3500 years. Within each soil, the four mineral-associated fractions display approximately the same residence time (34–42 years in 200 kyr soil, 29–37 years in 600 kyr soil, and 18–26 year in 1–3 Myr soils), indicating that a single stabilized SOM pool exists in these soils. For future use of $\Delta^{14}C$ to measure SOC turnover in similar soils, the use of FPOM is recommended to separate an active SOM pool from stabilized and passive mineral-associated SOM pools. The trend of decreasing stabilized SOM residence times as a function of soil age suggests that processes which release stabilized SOM from physical protection within soil aggregate structure are more abundant in the older soil. Candidates for processes that disrupt soil structure include burrowing fauna, clay shrink/swell activity, and the growth of plant roots and fungal hyphae. If the growth of plant roots and fungal hyphae play a role in stabilized SOM turnover, this effect could be included in ecosystem biogeochemistry models.

[52] **Acknowledgments.** We thank the graphite laboratory at CAMS for assistance with samples, as well as Mary Firestone and Teri C. Balser for ideas that helped this project develop. Julia Gaudinski and Jennifer Harden provided helpful suggestions for laboratory methods and field sampling, respectively. Carrie Masiello, Cristina Castahna, and two anonymous reviewers provided helpful reviews of earlier drafts. Funding for this work was provided by a NASA Earth System Science Fellowship to WTB, the Kearney Foundation for Soil Science, an LLNL-UC collaborative research program, and the University of California DANR.

References

Amundson, R., and W. T. Baisden, Stable isotope tracers and mathematical models in soil organic matter studies, in *Methods in Ecosystem Science*, edited by O. E. Sala et al., pp. 117–134, Springer–Verlag, New York, 2000.

Anderson, D. W., and E. A. Paul, Organo-mineral complexes and the study by radiocarbon dating, *Soil Sci. Soc. Am. J.*, *48*, 298–301, 1984.

Arkley, R. J., *Soil Survey of the Merced Area, California*, U.S.D.A. Soil Survey Serial, Washington, D. C., 1962.

Arkley, R. J., *Soil Survey of the Eastern Stanislaus Area, California*, U.S.D.A. Soil Survey Serial, Washington, D. C., 1964.

Baisden, W. T., R. G. Amundson, D. L. Brenner, A. C. Cook, C. Kendall, and J. Harden, A multi-isotope C and N modeling analysis of soil organic matter turnover and transport as a function of soil depth in a California annual grassland soil chronosequence, *Global Biogeochem. Cycles*, *16*, doi:10.1029/2001GB001823, in press, 2002.

Beare, M. H., M. L. Cabrera, P. F. Hendrix, and D. C. Coleman, Aggregate-protected and unprotected organic matter pools in conventional and no tillage soils, *Soil Sci. Soc. Am. J.*, *58*, 787–795, 1994.

Berger, R., Clean air $\Delta^{14}C$ from a California high desert site, *Radiocarbon*, *29*, 18–23, 1987.

Bevington, P. R., *Data Reduction and Error Analysis for the Physical Sciences*, 336 pp., McGraw-Hill, New York, 1969.

Brenner, D. L., W. T. Baisden, C. Kendall, J. Harden, and R. Amundson, Soil N and ^{15}N variation with time in a California Annual Grassland Ecosystem, *Geochim. Cosmochim. Acta*, *65*(22), 4171–4186, 2001.

Burke, I., C. Yonker, W. Parton, C. Cole, K. Flach, and D. Schimel, Texture, climate and cultivation effects on soil organic matter content in U.S. grassland soils, *Soil Sci. Soc. Am. J.*, *53*, 800–805, 1989.

Cambardella, C. A., and E. T. Elliott, Methods for physical separation and characterization of soil organic matter fractions, *Geoderma*, *56*(1–4), 449–457, 1993.

Cambardella, C. A., and E. T. Elliot, Carbon and nitrogen dynamics of soil organic matter fractions from cultivated grassland soils, *Soil Sci. Soc. Am. J.*, *58*, 123–130, 1994.

Carter, M. R., Analysis of soil organic matter storage in agroecosystems, in *Structure and Organic Matter Storage in Agricultural Soils*, edited by M. R. Carter and B. A. Stewart, pp. 3–14, CRC Press, Boca Raton, Fla., 1996.

Carter, M. R., and E. G. Gregorich, Methods to characterize and quantify organic matter storage in soil fractions and aggregates, in *Structure and Organic Matter Storage in Agroecosystems*, edited by M. R. Carter and B. A. Stewart, pp. 449–468, CRC Press, Boca Raton, Fla., 1996.

Carter, M. R., and B. A. Stewart, *Structure and Organic Matter Storage in Agricultural Soils*, 477 pp., CRC Press, Boca Raton, Fla., 1996.

Davidson, E. A., and I. L. Ackerman, Changes in soil carbon inventories following cultivation of previously untilled soils, *Biogeochemistry*, *20*, 161–193, 1993.

Elliott, E. T., Aggregate structure and carbon, nitrogen and phosphorus in native and cultivated soils, *Soil Sci. Soc. Am. J.*, *50*, 627–633, 1986.

Gaudinski, J. B., S. E. Trumbore, E. A. Davidson, and S. H. Zheng, Soil carbon cycling in a temperate forest: Radiocarbon-based estimates of residence times, sequestration rates and partitioning of fluxes, *Biogeochemistry*, *51*(1), 33–69, 2000.

Golchin, A., J. M. Oades, J. O. Skjemstad, and P. Clarke, Soil structure and carbon cycling, *Aust. J. Soil Res.*, *32*, 1043–1068, 1994a.

Golchin, A., J. M. Oades, J. O. Skjemstad, and P. Clarke, Study of free and occluded particulate organic matter in soils by solid state 13C CP/MAS NMR spectroscopy and scanning electron microscopy, *Aust. J. Soil. Res.*, *32*, 285–309, 1994b.

Golchin, A., P. Clarke, J. M. Oades, and J. O. Skjemstad, The effects of cultivation on the composition of organic matter and structural stability of soils, *Aust. J. Soil Res.*, *33*, 975–993, 1995a.

Golchin, A., J. M. Oades, J. O. Skjemstad, and P. Clarke, Structural and dynamic properties of soil organic matter as reflected by 13C natural abundance, pyrolysis mass spectrometry and solid state 13C NMR spectroscopy in density fractions of an oxisol under forest and pasture, *Aust. J. Soil Res.*, *33*, 59–76, 1995b.

Harden, J. W., *Soils Developed on Granitic Alluvium near Merced*, California, USGS, 1987.

Jenkinson, D. S., The turnover of organic carbon and nitrogen in soil, *Philos. Trans. R. Soc. London, Ser. B*, *329*, 361–368, 1990.

Jones, M. B., and R. G. Woodmansee, Biogeochemical cycling in annual grassland ecosystems, *Bot. Rev.*, *45*(2), 111–144, 1979.

Karlen, D. L., and C. Cambardella, Conservation strategies for improving soil quality and organic matter storage, in *Structure and Organic Matter Storage in Agroecosystems*, edited by M. R. Carter and B. A. Stewart, pp. 395–420, CRC Press, Boca Raton, Fla., 1996.

Kooistra, M. J., and M. van Noordwijk, Soil architecture and distribution of organic matter, in *Structure and Organic Matter Storage in Agroecosystems*, edited by M. R. Carter and B. A. Stewart, pp. 15–56, CRC Press, Boca Raton, Fla., 1996.

Lal, R., and J. M. Kimble, Conservation tillage for carbon sequestration, *Nutrient Cycling Agroecosystems*, *49*(1–3), 243–253, 1997.

Landsberg, J. J., and R. H. Waring, A generalised model of forest productivity using simplified concepts of radiation-use efficiency, carbon balance and partitioning, *For. Ecol. Manage.*, *95*, 209–228, 1997.

Levin, I., and B. Kromer, Twenty years of atmospheric (CO_2)-C-14 observations at Schauinsland station, Germany, *Radiocarbon*, *39*(2), 205–218, 1997.

Levin, I., B. Kromer, H. Schoch-Fischer, M. Bruns, M. Munnich, D. Berdau, J. C. Vogel, and K. O. Munnich, $\Delta^{14}CO_2$ record from Vermunt, in *Trends: A Compendium Of Data On Global Change,* Carbon Dioxide Information Analysis Center, Oak Ridge National Laboratory, Oak Ridge, TN, USA, 1994.

Marchand, D., and A. Allwardt, *Late Cenozoic Stratigraphic Units in The Northeastern San Joaquin Valley, California*, U.S.G.S. Bulletin, 1981.

Minagawa, M., D. Winter, and I. Kaplan, Comparison of Kjeldahl and combustion methods for measurement of nitrogen isotope ratios in organic matter, *Anal. Chem.*, *56*, 1859–1861, 1984.

Nadelhoffer, K., and B. Fry, Controls on natural nitrogen-15 and carbon-13 abundances in forest soil organic matter, *Soil Sci. Soc. Am. J.*, *52*, 1633–1640, 1988.

Nydal, R., and K. Lovseth, *Carbon-14 Measurements in Atmospheric CO_2 From Northern and Southern Hemisphere Sites, 1962–1993*, Oak Ridge National Laboratory, Oak Ridge, TN, USA, 1997.

Oades, J. M., An introduction to organic matter in mineral soils, in *Minerals in Soil Environments*, edited by J. B. Dixon and S. B. Weed, pp. 89–159, Soil Sci. Soc. of Am., Madison, Wis., 1989.

Oades, J. M., The role of biology in the formation, stabilization and degradation of soil structure, *Geoderma*, *56*, 377–400, 1993.

Oades, J., An overview of processes affecting the cycling of organic carbon in soils, in *The Role of Nonliving Organic Matter in the Earth's Carbon Cycle*, edited by R. Zepp and C. Sontagg, pp. 293–304, John Wiley, New York, 1995.

Oades, J. M., and A. G. Waters, Aggregate hierarchy in soils, *Aust. J. Soil Res.*, *29*, 815–828, 1991.

Parton, W. J., D. S. Schimel, C. V. Cole, and D. S. Ojima, Analysis of factors controlling soil organic matter levels in Great Plains grasslands, *Soil Sci. Soc. Am. J.*, *51*, 1173–1179, 1987.

Parton, W. J., D. S. Ojima, and D. S. Schimel, Models to evaluate soil organic matter storage and dynamics, in *Structure and Organic Matter Storage in Agroecosystems*, edited by M. R. Carter and B. A. Stewart, CRC Press, Boca Raton, Fla., 1996.

Paul, E., R. Follet, S. Leavitt, A. Halvorson, G. Peterson, and D. Lyon, Radiocarbon dating for determination of soil organic matter pool sizes and dynamics, *Soil Sci. Soc. Am. J.*, *61*, 1058–1068, 1997.

Schonhofer, F., C-14 in Austrian Wine and Vinegar, *Radiocarbon*, *34*(3), 768–771, 1992.

Six, J., R. Merckx, K. Kimpe, K. Paustian, and E. T. Elliott, A re-evaluation of the enriched labile soil organic matter fraction, *Eur. J. Soil Sci.*, *51*(2), 283–293, 2000.

Soil Survey Staff, *Soil Survey Manual*, U.S. Govt Print. Off., Washington, D. C., 1993.

Tiessen, H., E. Cuevas, and P. Chacon, The role of soil organic matter in sustaining soil fertility, *Nature*, *371*, 783–785, 1994.

Tisdall, J. M., and J. M. Oades, Organic matter and water-stable aggregates in soils, *J. Soil Sci.*, *33*, 141–163, 1982.

Torn, M. S., S. E. Trumbore, O. A. Chadwick, P. M. Vitousek, and D. M. Hendricks, Mineral control of soil organic carbon storage and turnover, *Nature*, *389*(6647), 170–173, 1997.

Trumbore, S. E., Comparison of carbon dynamics in tropical and temperate soils using radiocarbon measurements, *Global Biogeochem. Cycles*, *7*, 275–290, 1993.

Trumbore, S. E., Age of soil organic matter and soil respiration: Radiocarbon constraints on belowground dynamics, *Ecol. Appl.*, *10*(2), 399–411, 2000.

Trumbore, S. E., and S. Zheng, Comparison of fractionation methods for soil organic matter ^{14}C analysis, *Radiocarbon*, *38*, 219–229, 1996.

Trumbore, S., O. Chadwick, and R. Amundson, Rapid exchange between soil carbon and atmospheric carbon dioxide driven by temperature change, *Science*, *272*, 393–396, 1996.

VanVeen, J. A., and P. J. Kuikman, Soil structural aspects of decomposition of organic matter by micro-organisms, *Biogeochemistry*, *11*, 213–233, 1990.

White, A., A. Blum, M. Schulz, T. Bullen, J. Harden, and M. Peterson, Chemical weathering rates of a soil chronosequence on granitic alluvium, part I. Quantification of mineralogical and surface area changes and calculations of primary silicate reaction rates, *Geochim. Cosmochim. Acta*, *60*, 2533–2550, 1996.

R. Amundson and D. L. Brenner, Ecosystem Sciences Division, Department of ESPM, University of California, Berkeley, Berkeley, CA 94720, USA.

W. T. Baisden, Landcare Research, Massey University Campus, Private Bag 11052, Palmerston North, New Zealand. (BaisdenT@landcare.cri.nz)

A. C. Cook, Center for Accelerator Mass Spectrometry, Lawrence Livermore National Laboratory, Livermore, CA 94550, USA.